Supershear Rupture Propagation in a Monolithic Medium

K. Uenishi

Research Center for Urban Safety and Security, Kobe University, Kobe, Japan

1. Introduction

The rupture speeds obtained by fracture experiments of monolithic brittle linear elastic materials are usually by far lower than those predicted by theories and inferred from inversions of seismograms: The theoretical limiting propagation speed of a (continuously accelerating) crack tip is the Rayleigh wave speed c_R of the material under typical mode-I and II remote loading conditions. For mode-III loading, the theoretical limit is larger, the shear wave speed c_S of the medium, and some seismic inversions even suggest the existence of supershear rupture speeds (i.e., rupture propagating faster than the relevant shear wave; see Table 1) [1-5]. On the contrary, laboratory experiments and observations suggest that when a crack extends in brittle materials under suitable stress conditions and its velocity exceeds a certain limit, it oscillates (surface roughening) and subsequently divides into two or more branches. For a mode-I crack in brittle amorphous solids (glass, PMMA), the crack propagation speed c has experimentally an upper limit of order 0.5-$0.6c_S$ (0.55-$0.65c_R$). The fracture surface is mirror-smooth only for $c < 0.27$-$0.36c_S$ (0.3-$0.4c_R$). The crack surface roughens severely at higher speeds and the crack bifurcates at the highest speeds [6-9].

Table 1. Examples of earthquakes involving supershear fault rupture

Earthquake (year)	Rupture speed c [km/s]	S-wave speed c_S [km/s]	Mach number c/c_S
Imperial Valley, California (1979)	2.8	2.7-3.2	0.96-1.14
Landers, California (1992)	2.0	2.5-3.0	1.26-1.51
Izmit, Turkey (1999)	3.6	4.8-4.9	1.32-1.35
Central Kunlunshan, China (2001)	3.0-3.2	3.7-3.9	1.16-1.30
Denali, Alaska (2002)	3.1	3.3-3.5	1.06-1.13
Typical laboratory experiments	---	---	0.3-0.5

Correspondence footnote
Research Center for Urban Safety and Security, Kobe University
1-1 Rokko-dai, Nada, Kobe 657-8501 Japan
Fax: +81-78-803-6394 / Email: uenishi@kobe-u.ac.jp

Exceptionally, a few laboratory experiments of dynamic fracture on pre-cut interfaces do indicate that rupture propagating at the Rayleigh wave speed or larger can be found (e.g., [10, 11]), but the discrepancies of rupture speeds between theories and experiments (and numerical simulations) cannot always be attributed to the observations that real solids have every kind of defects such as pre-existing discontinuities or microcracks generated during rupture (crack) propagation, because similar inconsistencies may also appear in molecular-dynamics simulations of cracks propagating in perfect atomic lattices. Moreover, even when we accept the existence of such extraordinary high rupture speeds, the exact mechanism of rupture nucleation and the transition from sub-Rayleigh to supershear rupture speed has not been clarified yet, and the question of whether natural earthquake ruptures can propagate at such high speeds is still under active debate (see e.g., [12-15]).

Recent large-scale atomistic simulations show that hyperelasticity, the nonlinear elasticity of large strains, may be able to play a governing role in the dynamics of brittle fracture [16]. This is in contrast to many existing theories of dynamic fracture where the linear elasticity of solids is usually assumed to be sufficient to describe their mechanical behaviors. Real solids like the crust, however, have elastic properties that are significantly different at various scales, for both small and large deformations.

Here, in order to possibly explain the discrepancies described above, we experimentally investigate dynamic fracture in hyperelastic materials. Utilizing a high-speed digital video camera system, we record mode-I rupture initiation and dynamic propagation process. We shall show that if the magnitude of static crack-parallel (T-) stress is comparable to that of remote mode-I loading stress, the rupture propagates surprisingly straight and, even without the existence of material heterogeneities, the rupture front accelerates from zero to a constant supershear speed to capture the shear wave front generated upon rupture initiation.

2. Experimental Setup

As a first step toward further understanding of the effect of hyperelasticity on high-speed rupture initiation and propagation, we consider a typical hyperelastic medium, flat sheets of rubber (100mm high × 200mm wide or larger), stretched under static mode I loading conditions with crack-parallel T-stresses. Rupture (crack) is initiated by pricking the rubber sheet (Fig.1). The rupture initiation and dynamic propagation process is recorded and analyzed utilizing a high-speed digital video camera at a rate of 24,000 frames per second (i.e., at an interval of 41.7μs (41.7×10^{-6} sec)). The size of each digital image, taken during the observation duration of 1.365 sec, is 512×128 pixels.

The dots in Fig.1 mark grid points at intervals of 10 mm in the initial, statically stretched state. They are prepared for the observational purpose. We define the *x*-
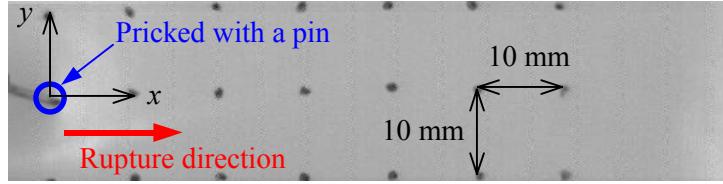
Fig.1. The definition of *x*- and *y*-axes. The rupture is initiated by prick of a pin and propagated in the *x*- direction of the hyperelastic rubber sheet.
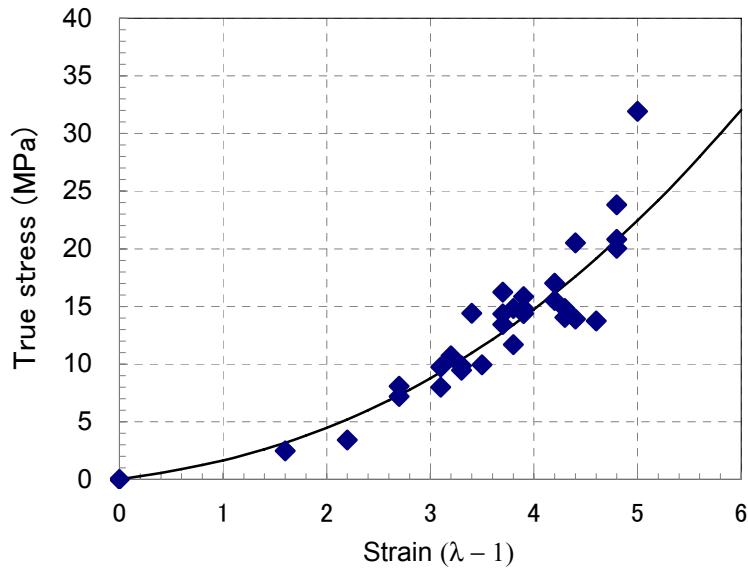
Fig.2. The true stress-strain relation of the rubber under biaxial loading ($\lambda_x = \lambda_y = \lambda$). The experimentally obtained result is indicated by dots. We notice rather strong strain-hardening effect. The solid curve is drawn for the theoretical stress-strain relation in the Generalized Neo-Hookean (GNH) model, with the shear modulus $\mu = 0.3$ MPa, "yielding" parameter $b = 1$ and the "hardening" parameter $n = 1.15$.

and *y*-axes as indicated in Fig.1: The *x*-axis corresponds to the direction of rupture propagation. We further define the extension ratio λ as the ratio of the deformed length to the undeformed length. Thus $\lambda_x = 1$ corresponds to the state where no deformation is found in the *x*-direction. The extension ratios λ_x and λ_y are related to the *T*-stress and mode-I loading, respectively.

We conduct over 100 dynamic rupture experiments under different extension ratios (λ_x: 1.0-5.8, λ_y: 2.2-7.0), and before performing the dynamic experiments,

we measure and plot the true (Cauchy) stress-strain relation under static biaxial conditions. The result is depicted in Fig.2. The term "hyperelasticity" is often associated with a nonlinear "strain-softening" relation, but in Fig.2, like in [17], the rubber clearly shows a nonlinear "strain-hardening" behavior. This relation roughly corresponds to that in the Generalized Neo-Hookean (GNH) model where, upon modification of the results found in [18], the true stress τ may be expressed as $\tau = \mu \left[2\lambda^2 + b \left(2\lambda^2 + 1/\lambda^2 - 3 \right) / n \right]^{n-1} \left(\lambda^2 - 1/\lambda^2 \right)$, with the shear modulus μ, "hardening" parameter n and "yielding" parameter b (solid line in Fig.2). In [18], it is shown that the "hardening" parameter n greater than 1/2 gives a positive slope of the stress-strain curve and renders the elliptic situation of the problem, at least for the case of engineering (nominal) uniaxial stress.

3. Subsonic and Supershear Rupture Propagation in a Hyperelastic Medium

First, we apply relatively small crack-parallel T-stresses (strains), λ_x. The experimentally obtained photographs are shown in Fig.3 for the case of uniaxial tension in the y-direction, $\lambda_y = 3.0$. In the relatively small (or zero) static T-stress range, upon initiation, the rupture surfaces form an elliptical shape because large deformations are allowed in hyperelastic materials (see the inside of the red ellipse in Fig.3(a)). Then, the rupture propagates relatively slowly, wriggles or bifurcates, leaving a wavy pattern on the edges of the ruptured fragments. The diagram showing the relation between the speed and front position of rupture (Fig.4) suggests that the rupture speed rapidly increases after initiation to approach a constant value. In this low T-stress case, it is difficult to identify sound waves in the recorded pictures, but considering the deformation patterns in Fig.3, the rupture speed itself is very low and seems to be still in a subsonic range.

(a) 2.041 ms (2.041×10^{-3} sec)   (c) 8.083 ms

(b) 5.666 ms   (d) 10.083 ms
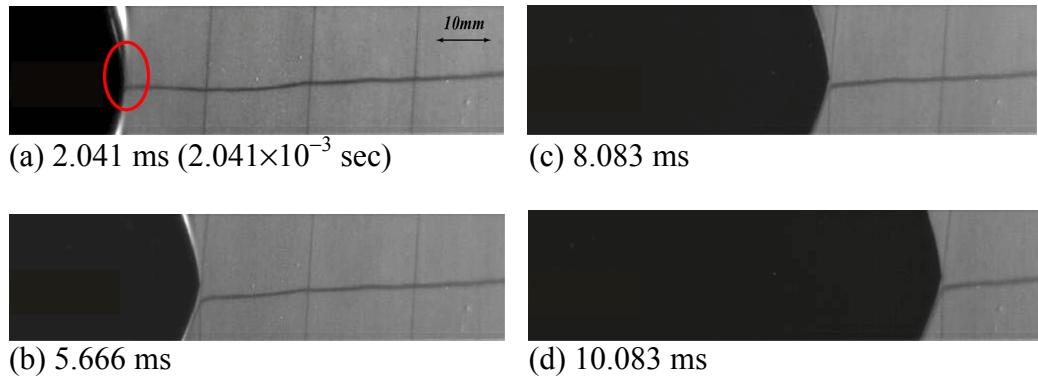
Fig.3. Typical hyperelastic dynamic rupture propagation recorded experimentally utilizing a high-speed digital video camera (under uniaxial tension; extension ratio: $\lambda_y = 3.0$; final rupture speed: 11 m/s). Elapsed time after rupture initiation is indicated in milliseconds. The initial thickness of the rubber sheet is 1 mm and the lines are drawn for the observational purpose.
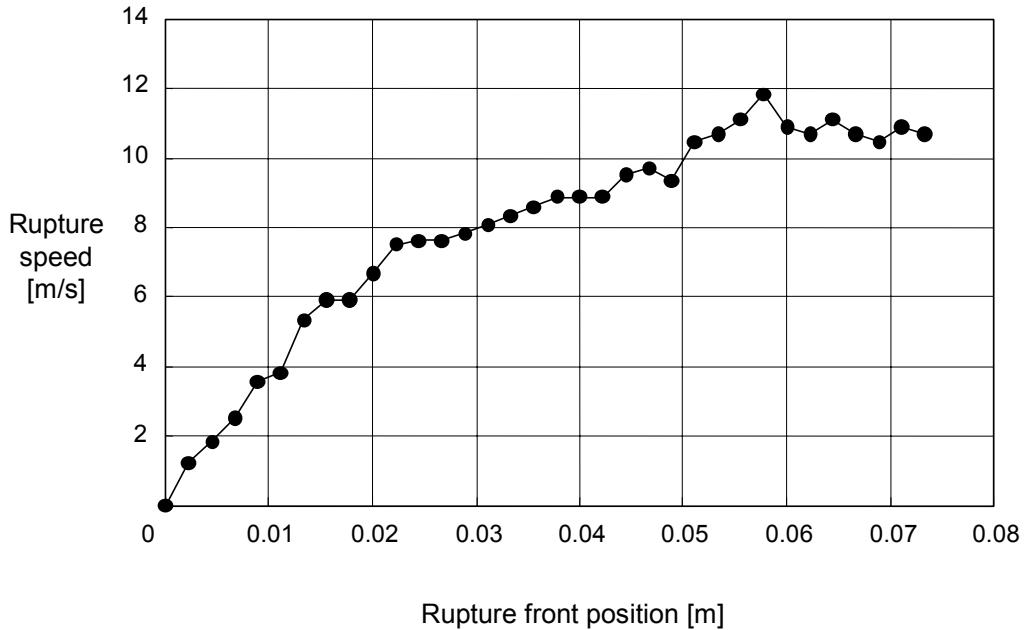
Fig.4. History of the speed of the rupture front: Subsonic case. Upon initiation, the rupture speed increases fast and approaches a constant value.

Second, we increase the values of both extension ratios, λ_x and λ_y. In monolithic brittle elastic materials, T-stress is known to have the stabilizing effect on rupture propagation [9]. The results here show that similar effects can be generally observed in the hyperelastic case, but the dynamic rupture behavior is more sensitive to the static loading conditions in the hyperelastic case than in the linear elastic case. If the magnitude of the static T-stress is comparable to that of the remote mode-I loading stress (Fig.5), the rupture propagates straight and rupture front, forming a very sharp wedge-shape, accelerates from zero to a constant supershear speed (Fig.6) and then captures the shear wave front generated upon rupture initiation (directly shown in Fig.5(d)-(f)). The final, constant propagation speed is largely controlled by the static T-stress (λ_x) as well as λ_y (Fig.7). Sound (shear) waves can be clearly identified in the recorded photographs, and in Fig.5, wave fronts are indicated by red broken lines. In Fig.8, values of wave speeds are shown for various extension ratios, λ_x and λ_y, where we find that larger extension ratios generally give greater wave speeds. This is expected from the steeper slope of the nonlinear stress-strain curve in a higher range of extension ratio (Fig.2). In Fig.9, we notice that the Mach numbers (here, the ratio of rupture speed to shear wave speed) can often exceed 2 and the seismologically observed values (~ 1; Table 1) are, at least from hyperelastic mode-I point of view, not extraordinarily high.

5

(a) 0 µs

(b) 41.7 µs (41.7×10^{-6} sec)

(c) 83.3 µs

(d) 125.0 µs

(e) 166.7 µs

(f) 208.3 µs

(g) 250.0 µs

(h) 291.7 µs

(i) 333.3 µs

(j) 375.0 µs

(k) 416.7 µs

(l) 458.3 µs
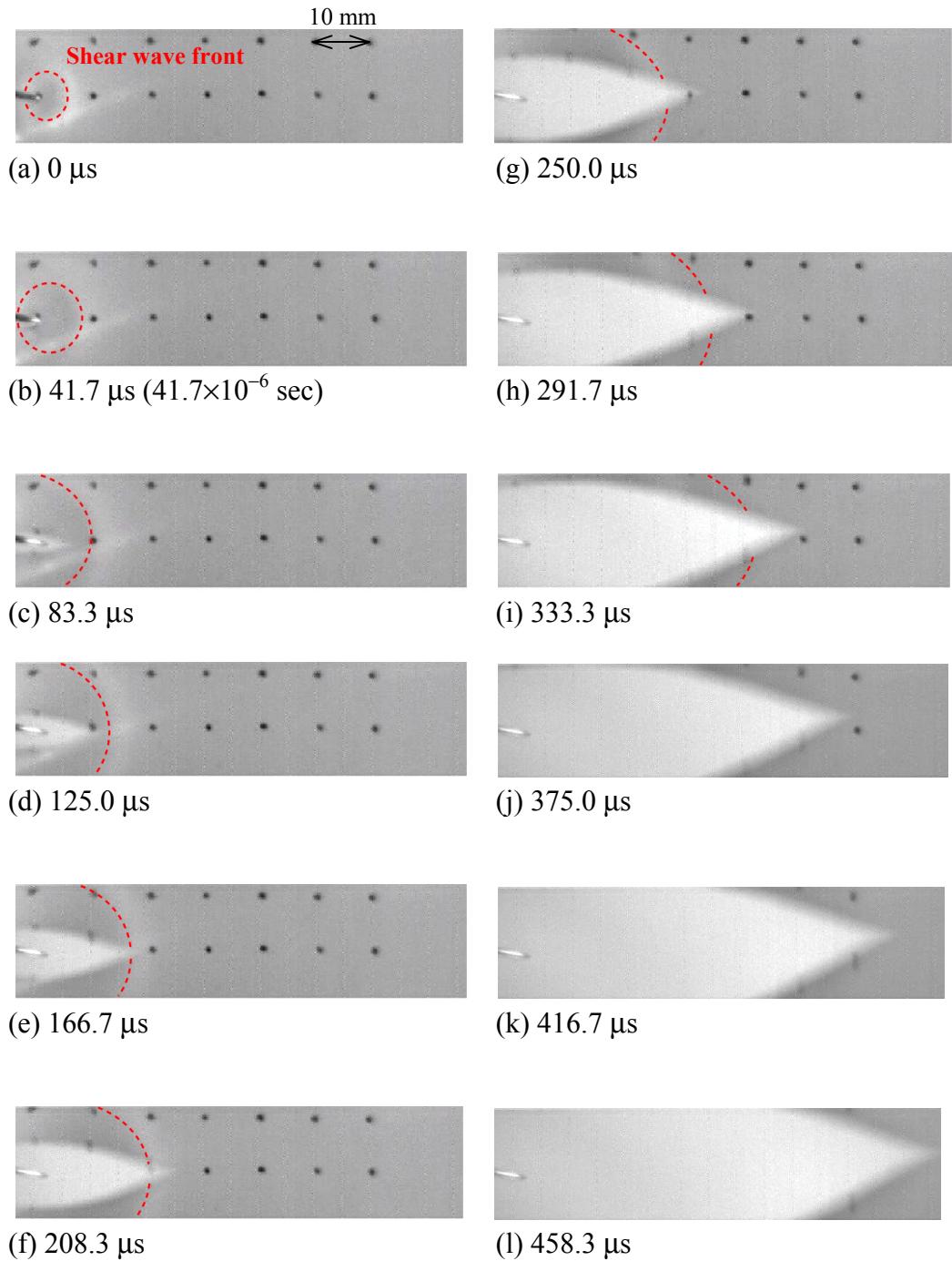
Fig.5. The dynamic rupture process recorded by the high-speed digital video camera system. These photographs show that the rupture speed becomes larger than the (shear) wave speed (extension ratios: $\lambda_x = 4.0$, $\lambda_y = 4.0$; final rupture speed: 181 m/s; wave speed: 75 m/s; initial thickness of the rubber 2.2 mm). The red broken lines correspond to the wave fronts. Elapsed time after rupture initiation is given in microseconds.
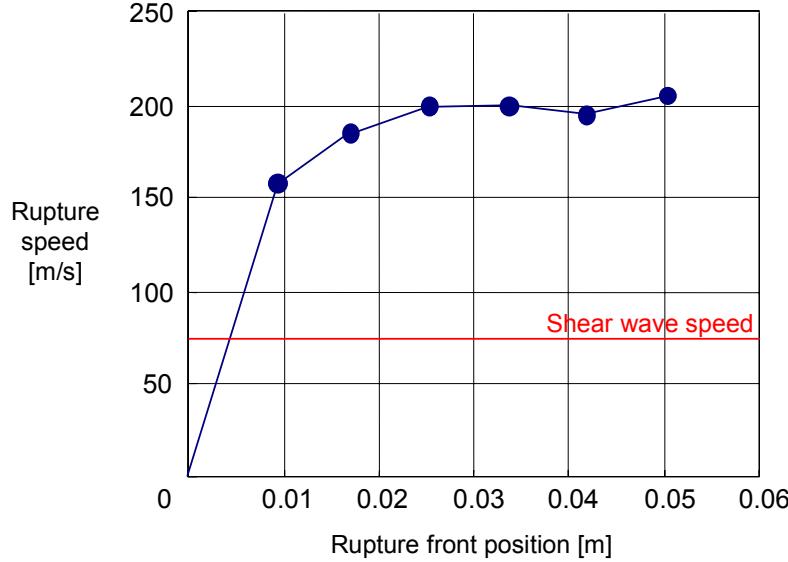
Fig.6. History of rupture speed: Supershear case. Similar to the subsonic case, the rupture speed increases immediately after initiation and approaches a final constant value exceeding the shear wave speed.
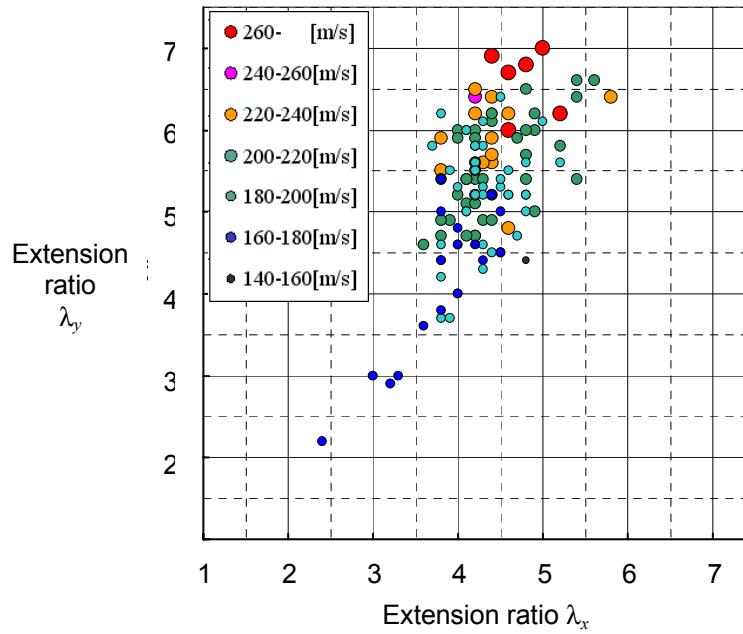
Fig.7. The (final constant) speed of stably propagating rupture under various extension ratios. Similar to the linear elastic case, higher T-stress (λ_x) generally gives more stability of rupture propagation and thus renders larger rupture speed, but the extension ratio λ_y, measured perpendicular to the rupture direction, has also strong influence on the propagation speed.
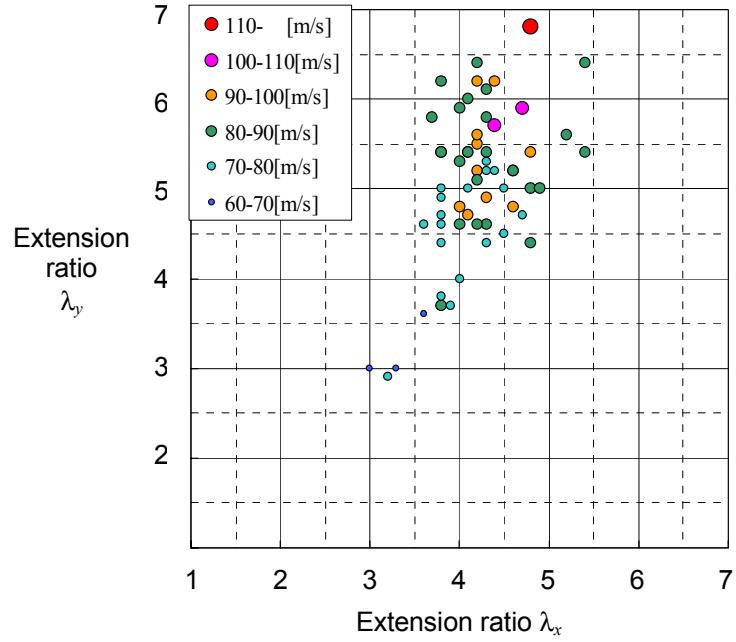
Fig.8.　The experimentally observed shear wave speeds under different combinations of extension ratios. As can be expected from the nonlinear stress-strain relation shown in Fig.2, higher extension ratios generally give larger wave speed.
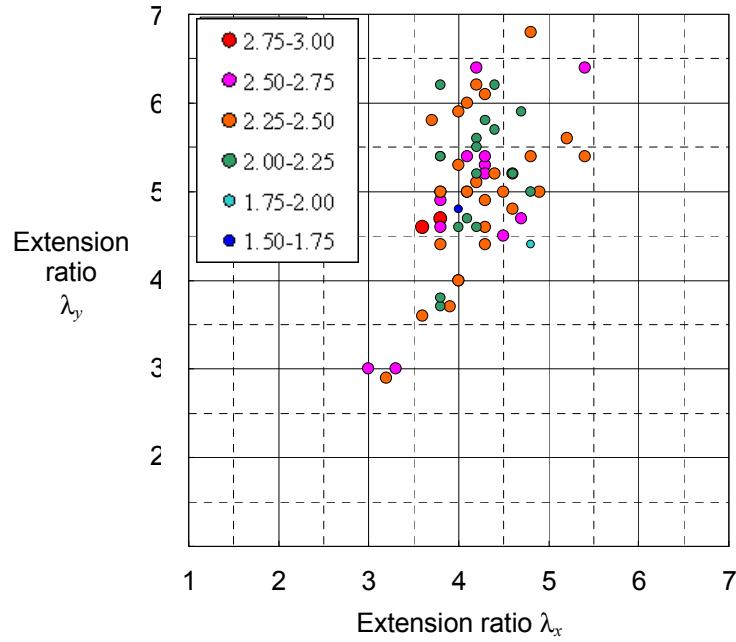
Fig.9.　The Mach numbers (the ratio of rupture speed to shear wave speed) obtained experimentally in a monolithic medium, under different extension ratios. In hyperelastic media, Mach numbers over 2 can be commonly observed.

These experimental results suggest – if the hyperelastic constitutive relation such as shown in Fig.2 can be assumed – rupture may reach supershear speed even when material heterogeneities do not exist. This is totally different from the conventional interpretation of rupture of geological faults where pre-cut or dissimilar interfaces are usually assumed in order to explain the "extraordinary" high rupture speed. Although strain-softening behavior may prevail in crustal rocks under quasi-static loading, dynamic loading (and higher strain rate of loading, e.g., due to detonation by blasting) gives strain-hardening effect on rocks (see, for example, [19] and references therein). Therefore, the laboratory observations described here might possibly give a new hint on the question of whether natural earthquake ruptures can really accelerate to such "extraordinary" high speeds as have been inferred from seismological inversions.

4. Conclusions

In order to possibly explain the discrepancies between the rupture speeds obtained or inferred from laboratory experiments, theories and seismological observations, we experimentally investigated dynamic fracture in hyperelastic materials. The result shows that the dynamic rupture (crack) behavior is more sensitive to the static loading conditions in the hyperelastic case than in the linear elastic case: If the static *T*-stress is relatively small, upon rupture initiation, the rupture surfaces form an elliptical shape and propagate relatively slowly, leaving a wavy pattern of the ruptured surfaces; If the static *T*-stress is comparable to the remote mode-I loading stress, the rupture propagates straight and rupture front forms a very sharp wedge-shape to accelerate to a constant supershear speed (Mach numbers over 2), even when there is no initial material heterogeneity. This result might be consistent with the "extraordinary" high speeds expected from seismological observations and give a new interpretation of the physical properties of the media surrounding geological faults.

References

[1]   P. Spudich, E. Cranswick, Direct observation of rupture propagation during the 1979 Imperial Valley earthquake using a short beseline accelerometer array, Bull Seism Soc Am, 74(6) (1984) 2083-2114.

[2]   K.B. Olsen, R. Madariaga, R.J. Archuleta, Three-dimensional dynamic simulation of the 1992 Landers earthquake, Science, 278(5339) (1997) 834-838.

[3]   M. Bouchon, M.N. Toksöz, H. Karabulut, M.-P. Bouin, M. Dietrich, M. Aktar, M. Edie, Space and time evolution of rupture and faulting during the 1999 Izmit (Turkey) earthquake, Bull Seism Soc Am, 92(1) (2002) 256-266.

[4]   M. Bouchon, M. Vallée, Observation of long supershear rupture during the magnitude 8.1 Kunlunshan earthquake, Science, 301(5634) (2003) 824-826.

[5] D.D. Oglesby, D.S. Dreger, R.A. Harris, N. Ratchkovski, R. Hansen, Inverse kinematic and forward dynamic models of the 2002 Denali Fault earthquake, Alaska, Bull Seism Soc Am, 94(6B) (2004) S214-S233.

[6] K. Ravi-Chandar, W.G. Knauss, An experimental investigation into dynamic fracture. I. Crack initiation and crack arrest; II. Microstructural aspects; III. Steady state crack propagation and crack branching; IV. On the interaction of stress waves with propagating cracks, Int J Fracture, 25 (1984) 247-262; 26 (1984) 65-80; 141-154; 189-200.

[7] E. Sharon, J. Fineberg, Microbranching instability and the dynamic fracture of brittle materials, Phys Rev B, 54 (1996) 7128-7139.

[8] J.R. Rice, New perspectives on crack and fault dynamics, in: H. Aref, J.W. Phillips (Eds.), Mechanics for a New Millennium, Kluwer Academic Publishers, Dordrecht, 2001, pp.1-23.

[9] K. Uenishi, H.P. Rossmanith, Stability of dynamically propagating cracks in brittle materials, Acta Mech, 156(3-4) (2002) 179-192.

[10] K. Uenishi, H.P. Rossmanith, A.E. Scheidegger, Rayleigh pulse − dynamic triggering of fault slip, Bull Seism Soc Am, 89(5) (1999) 1296-1312.

[11] A.J. Rosakis, Intersonic shear cracks and fault ruptures, Adv Phys, 51 (2002) 1189-1257.

[12] R.D. Deegan, P.J. Petersan, M. Marder, H.L. Swinney, Oscillating fracture paths in rubber, Phys Rev Lett, 88(1) (2002) Doi: 10.1103/PhysRevLett.88. 014304.

[13] K. Xia, A.J. Rosakis, H. Kanamori, Laboratory earthquakes: the sub-Rayleigh-to-supershear rupture transition, Science, 303 (2004) 1859-1861.

[14] K. Uenishi, Supershear rupture propagation in homogeneous, monolithic media: experimental observations. Eos Trans AGU, 87(52) (2006) Fall Meet Suppl Abstract S33C-03.

[15] S. Das, The need to study speed, Science, 317 (2007) 905-906.

[16] M.J. Buehler, H. Gao, Dynamical fracture instabilities due to local hyperelasticity at crack tips, Nature, 439 (2006) 307-310.

[17] A. Stevenson, A.G. Thomas, On the bursting of a balloon, J Phys D: Appl Phys, 12(12) (1979) 2101-2109.

[18] P.H. Geubelle, W.G. Knauss, Finite strains at the tip of a crack in a sheet of hyperelastic material: I. Homogeneous case, J. Elasticity, 35 (1994) 61-98.

[19] X. Zhou, Q. Hac, Y. Zhanga, K. Zhua, Analysis of deformation localization and the complete stress-strain relation for brittle rock subjected to dynamic compressive loads, Int J Rock Mech & Min Sci, 41 (2004) 311-319.